ACADEMIC PRESS

Journal of Solid State Chemistry 169 (2002) 131–138

JOURNAL OF SOLID STATE CHEMISTRY

www.academicpress.com

$PbMnO_{2.75}$—a high-pressure phase having a new type of crystallographic shear structure derived from perovskite

C. Bougerol,[a] M.F. Gorius,[a] and I.E. Grey[b,*]

[a] *CNRS Laboratoire de Cristallographie, BP166, 38042 Grenoble, France*
[b] *CSIRO Minerals, Box 312, Clayton South, Vic. 3169, Australia*

Received 20 June 2002; accepted 25 September 2002

Abstract

$PbMnO_{2.75}$, prepared at 7.8 GPa and 880°C, has monoclinic symmetry, $A2/m$, with cell parameters $a = 32.232(5))$ Å, $b = 3.831(1))$ Å, $c = 35.671(5)$ Å, $\beta = 130.00(1)°$. Electron diffraction patterns of the phase show features characteristic of ReO_3-based crystallographic shear (CS) structures, and a model for the structure was developed on this basis which gave a good fit to powder X-ray diffraction and neutron diffraction patterns. The structure can be formally derived from the perovskite structure by periodic shear on $(704)_p$ planes, giving blocks of perovskite that are displaced relative to one another by the CS vector of $\frac{1}{2}[110]_p$. Ordered oxygen vacancies occur at the CS planes which convert the MnO_6 octahedra to MnO_5 square pyramids, resulting in the formation of pseudo-hexagonal channels along [010]. Pb atoms occupy these channels and form pyramidal coordination to oxygen. The PbO_4 pyramids edge-share with the MnO_5 square pyramids to form elements with the topology of tetragonal PbO. Pb atoms also occupy the *A*-cation sites in the perovskite blocks. This is the first example of a structure based on CS of the ReO_3 structure where the *A*-cation sites are occupied, thus giving a perovskite CS phase.

1. Introduction

Perovskite-type oxide phases containing manganese in the *B*-cation sites have been intensively studied in recent years because of their unusual magnetic and electric properties. These include large magnetoresistive effects, nanoscale charge ordering, magnetic field dependence of phase transitions and high oxygen ion conductivity, all of which have potentially important device applications [1–4]. The properties can be controlled by *A*-cation site doping to change the Mn^{3+}/Mn^{4+} ratio. Properties such as charge ordering can also be strongly influenced and controlled by substitution of large cations possessing electron lone pairs in the *A*-cation sites. The highest charge ordering temperature reported for manganites (475 K) occurs for $Bi_{0.5}Sr_{0.5}MnO_3$ and has been attributed to the effect of the Bi^{3+} $6s^2$ lone pair electrons on the mobility of the charge carriers [5].

Divalent lead also has a $6s^2$ lone pair configuration, but no manganite perovskites have been reported with Pb^{2+} as the *A*-site cation. The characterized phases in the $PbO–MnO_2–Mn_2O_3$ system are Pb_2MnO_4 [6], a hollandite-type mineral of approximate composition $PbMn_8O_{16}$ [7], and $Pb_3Mn_7O_{15}$, with a structure based on a hexagonally close-packed (O + Pb) framework and with Mn in octahedral interstices [8]. A number of other compositions have been reported but not characterized which are probably cation-deficient variations of the $Pb_3Mn_7O_{15}$ phase type [9]. The above phases are all stable at ambient pressure. Since $BiMnO_3$ can only be prepared at high pressures [10], we undertook an investigation of the $PbO–MnO_2–Mn_2O_3$ system at elevated pressures to see if perovskite-type phases could be synthesized. Two new perovskite-related phases were found to be stable at a pressure of ~8 GPa; $PbMnO_3$ [11] with a monoclinically distorted 6H-$BaTiO_3$-type structure [12], and $PbMnO_{2.75}$ with a structure derived from perovskite by crystallographic shear (CS), which is the subject of this report.

2. Experimental

Starting materials for the preparation were PbO (Aldrich 99.9%), reagent-grade MnO_2, and Mn_2O_3 prepared by controlled reduction of MnO_2 in air at 800°C for 16 h. Ground mixtures of the starting

*Corresponding author. Fax: +3-9562-8919.
E-mail address: ian.grey@csiro.au (I.E. Grey).

0022-4596/02/$ - see front matter © 2002 Elsevier Science (USA). All rights reserved.
PII: S0022-4596(02)00065-8

products were encased in a gold capsule (diameter 3 mm, height 6 mm) and placed in a tubular graphite heater. Pyrophillite was used as a pressure-transferring medium in a belt-type high-pressure reactor. From experience it was found that the reaction was achieved in less than 2 h. Most samples were reacted for 3 h.

Electron diffraction studies on crushed products were made using a Philips CM300 transmission electron microscope operated at 300 kV, with a Cs coefficient of 1.2 mm. Studies were made on thin edges of crystals produced by fracturing. Quantitative energy dispersive X-ray analyses were conducted using a beam current of 7.4 pA, an acquisition time of 100 s, a sample tilt angle of 20° and a takeoff angle of 30°. The data were processed using the Kevex Sigma EDX program.

Powder X-ray diffraction (XRD) data were collected on finely ground specimens using a Siemen's D5000 diffractometer, operated in transmission mode employing copper radiation. The Rietveld data collection was made in the 2θ range 10–90° using a step interval of 0.016° and a count time of 11 s per step. Neutron diffraction (ND) data sets were collected on a 100 mg sample using the D20 2-axis powder diffractometer [13] at the Institut Laue Langevin, Grenoble. Data were collected using a wavelength of 1.3 Å.

Refinements of the powder XRD and ND data were made using the Rietveld program SR5, a local modification of the code by Hill and Howard [14] and Wiles and Young [15]. A pseudo-Voigt peak shape function was employed together with a three-term width function and a four-parameter polynomial for the background.

3. Results and discussion

3.1. Syntheses

A 1:1 molar mixture of PbO and MnO_2 gave a single-phase product when reacted at 7.8 GPa and 880°C. The XRD powder pattern could be indexed using a monoclinic distortion of the 6H $BaTiO_3$ cell and a satisfactory Rietveld refinement of the structure was obtained on this basis [11]. When the reaction was carried out at a higher temperature of 1130°C, the XRD pattern showed that the 6H phase had decomposed to give PbO and $Pb_3Mn_4O_{15}$ together with peaks due to a new phase. Peaks due to the new phase were also found when the pressure was decreased to 4 GPa while maintaining the temperature at 880°C.

The new phase was prepared in an almost pure state by reacting a mixture of $PbO + 0.5MnO_2 + 0.5MnO_{1.5}$ ($= PbMnO_{2.75}$) at 7.8 GPa and 880°C for 3 h. Quantitative X-ray analyses on individual crystal of the new phase in the electron microscope gave average weight percent results of 20.7% Mn, 79.3% Pb, corresponding to an atomic ratio of [Mn]:[Pb] of 0.98. When the same starting mixture was reacted at a lower pressure of 4 GPa at 880°C a mixture of PbO and $Pb_3Mn_7O_{15}$ was obtained. Under ambient pressure conditions, reaction in air of the $PbMnO_{2.75}$ mixture gave a mixture of Pb_2MnO_4 and $Pb_3Mn_7O_{17}$. Our XRD pattern of this mixed-phase product agrees with that reported as single-phase $Pb_6Mn_6O_{17}$, prepared under the same conditions by Bush et al. [16], indicating that they had prepared a mixture of phases.

3.2. Diffraction data for $PbMnO_{2.75}$

The powder XRD pattern for $PbMnO_{2.75}$ is given in Table 1. Attempts to index the pattern using a number of different automatic indexing programs all failed. Electron diffraction patterns were then taken for the new phase. They showed that the phase had a simple 3.85 Å axis typical of perovskites, but the diffraction pattern obtained in projection down this axis was complex, comprising a series of parallel, closely spaced rows of reflections as illustrated in Fig. 1. The center-of-mass of the strongest reflections in each row defines a distorted 3.85×3.85 Å perovskite subcell, as illustrated by the large circles in Fig. 1. Careful measurements made on the ED pattern showed that the rows were oriented along $\mathbf{g}(704)_p$. The subscript p refers to a primitive cubic subcell common to the perovskite and ReO_3 structures. The ED section could be completely indexed using $a = 32.2$ Å, $c = 17.8$ Å and $\beta = 130°$.

ED patterns obtained by rotation away from the section shown in Fig. 1 were consistent with a monoclinic cell with $b = 3.85$ Å. However, the long axes

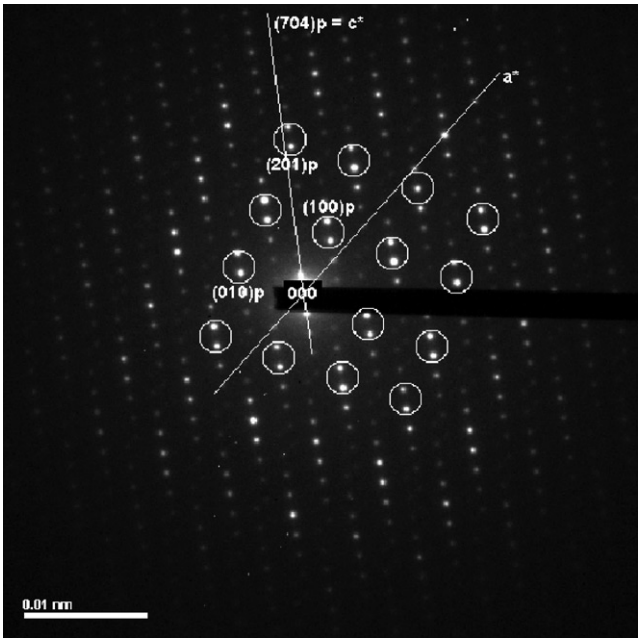

Fig. 1. [010] zone electron diffraction pattern for $PbMnO_{2.75}$.

Table 1
XRD powder pattern for $PbMnO_{2.75}$ prepared at 7.8 GPa and 880°C

d spacing	Intensity (rel)	hkl[a]
4.621	3	4 0 2
4.104	12	7 0 $\bar{8}$
3.794	14	0 1 1
3.577	15	4 0 4
3.515	6	7 0 $\overline{10}$
2.876	36	11 0 $\bar{6}$
2.781	100	4 1 3
2.702	63	7 1 $\bar{9}$
2.682	42	3 0 $\overline{12}$
2.344	12	3 1 $\overline{11}$
2.319	2	11 1 $\bar{7}$, 11 1 $\bar{9}$
2.263	26	11 1 $\bar{5}$
2.063	8	3 1 $\overline{13}$
2.052	7	14 0 $\overline{16}$
2.022	17	8 0 6
1.915	34	0 2 0
1.906	10	14 0 $\overline{18}$
1.785	4	8 0 8, 18 0 $\overline{14}$
1.776	3	15 0 $\bar{2}$, 10 0 $\overline{20}$
1.759	5	14 1 $\overline{17}$
1.736	3	7 2 $\bar{8}$
1.702	5	8 1 7
1.689	4	4 2 4
1.659	8	15 1 $\bar{3}$
1.622	4	18 1 $\overline{13}$
1.609	7	18 1 $\overline{15}$
1.594	13	11 2 $\bar{6}$
1.582	10	1 1 15
1.559	12	3 2 $\overline{12}$
1.538	9	10 1 $\overline{21}$
1.401	4	22 0 $\overline{10}$, 14 2 $\overline{16}$
1.391	10	8 2 6
1.351	4	14 2 $\overline{18}$
1.341	3	6 0 $\overline{24}$
1.333	3	22 1 $\overline{11}$
1.306	3	18 2 $\overline{14}$
1.301	3	15 2 $\bar{2}$, 10 2 $\overline{20}$
1.272	2	12 1 9
1.243	2	5 0 18, 1 2 16
1.218	7	4 3 3
1.211	5	7 3 $\bar{9}$

[a] Indices are for strongest reflections from Rietveld refinement of structure.
Refined cell parameters are $a = 32.232$ Å (5), $b = 3.831$ Å (1), $c = 35.671$ (5) Å, $\beta = 130.00$ (1)°.

involved and the relatively imprecise determination of the microscope stage rotation angles prevented a discrimination between a primitive cell ($P2/m$ or non-centrosymmetric subgroups) and a centered cell (which would require a doubling of one or both of the long axes).

3.3. Structural models

3.3.1. $\frac{1}{2}[1\ 0\ \bar{1}](704)_p$ CS model

The large unit cell for $PbMnO_{2.75}$, with the associated high degree of overlap of reflections in the powder patterns, prevented an ab initio structure determination. However, the [010] zone axis ED pattern has a strong resemblance to reported ED patterns for ReO_3-related CS structures [17]. This information, coupled with the relative simplicity of a short projection axis along [010], rendered feasible the derivation of a model by a crystal chemical approach. The cell dimensions define both the CS plane orientation and the spacing between CS planes. Together with the monoclinic symmetry and chemical composition information, this strongly limits the number of structural models to be tested against the powder diffraction data.

The measured CS plane orientation of $(704)_p$ is close to $(201)_p$, which is one of the principal CS planes in ReO_3-type CS structures. Compounds $(Mo,W)O_{3-x}$ form homologous series of $(201)_p$ CS structures, M_nO_{3n-1}, n integer, known as Magneli phases, after A. Magneli who first characterized them [18]. These phases can be formally generated from the ReO_3 structure type by removal of oxygen atoms along the CS planes followed by displacement of adjacent ReO_3-type blocks across the CS plane by the vector $\frac{1}{2}[1\ 0\ \bar{1}]_p$. The octahedral articulation changes from corner-sharing to edge-sharing at the CS boundaries. The plane $(704)_p$ found in $PbMnO_{2.75}$ can be written as $3(201)_p + (101)_p$. The operation $\frac{1}{2}[1\ 0\ \bar{1}](101)_p$ is an anti-phase boundary operation and it leaves the composition unchanged at the boundary.

A model was constructed for $PbMnO_{2.75}$ based on Magneli-type CS phases with a CS operation $\frac{1}{2}[1\ 0\ \bar{1}](704)_p$. It can be defined in the space group $P2/m$, which is a common space group for Magneli phases. The model is shown in Fig. 2, with the edge-shared octahedra at the CS planes shown with dark shading. The Mn atoms were ordered into the octahedral sites and Pb atoms were located in the A-type cavities. A

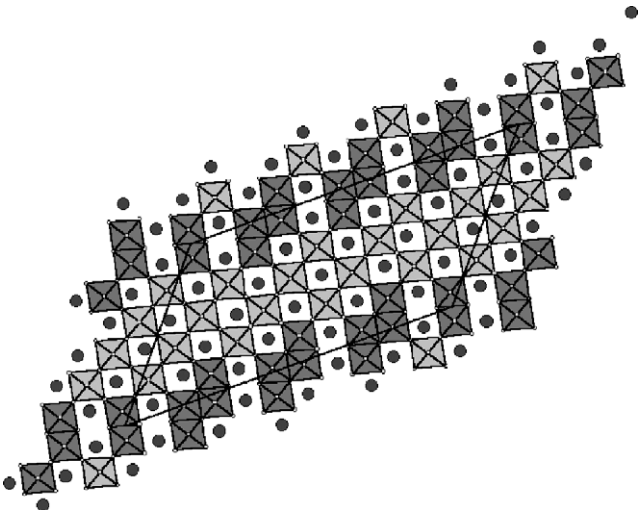

Fig. 2. [010] projection of CS model generated by the CS operation $\frac{1}{2}[1\ 0\ \bar{1}](704)_p$ on perovskite. Dark shading corresponds to edge-shared octahedra at CS boundaries. Filled circles are Pb atoms.

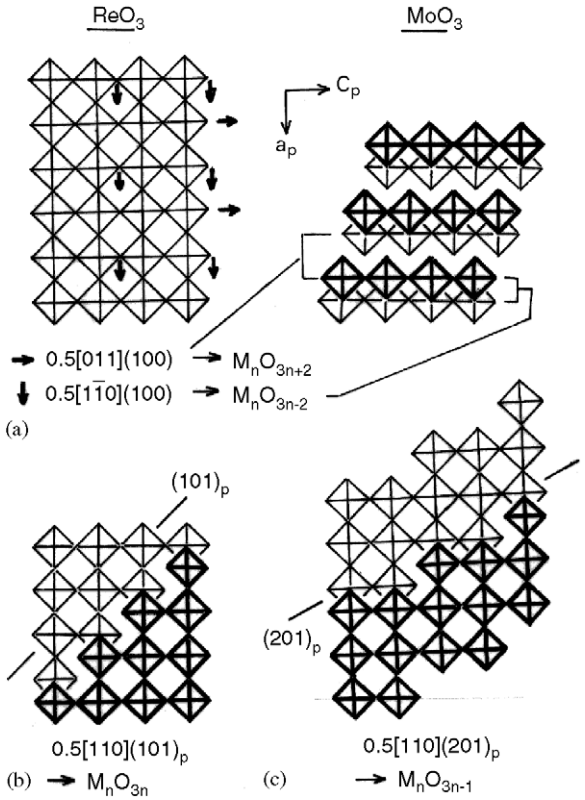

Fig. 3. (a) Formation of MoO_3 structure from ReO_3 structure by application of CS vectors $\frac{1}{2}[011]_p$ and $\frac{1}{2}[110]_p$ to alternate $(100)_p$ planes. (b) CS plane generated by the operation $\frac{1}{2}[110](101)_p$. (c) CS plane generated by the operation $\frac{1}{2}[110](201)_p$.

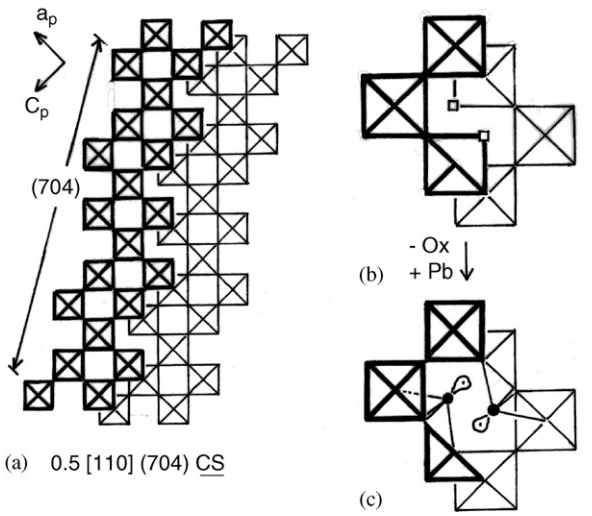

Fig. 4. (a) CS plane generated by the operation $\frac{1}{2}[110](704)_p$ on perovskite. (b). Enlargement of part of CS boundary showing removal of non-bridging oxygen atoms to generate six-sided channels. (c). Location of Pb atoms in channels showing pyramidal bonds to oxygen atoms and the direction of their $6s^2$ lone electron pairs.

powder pattern calculated from the model gave reasonable agreement with the experimental model for $(h0l)$ reflections indicating that the structure projected along b was approximately correct. However, very poor agreement was obtained for reflections with $k \neq 0$. A serious deficiency with the model was that the calculated c parameter, based on an ideal ReO_3 subcell with $a_p = 3.85$ Å, is considerably larger (18.3 Å) than the measured c parameter (17.8 Å). This is counter to published information on $(h0l)_p$ CS structures for which measured a and c parameters are always larger than the values calculated from an ideal ReO_3 subcell, due to octahedral distortions associated with repulsions of M atoms across shared octahedral edges at the CS planes. This model was thus discarded and alternative types of CS operations were considered.

3.3.2. $\frac{1}{2}[110](704)_p$ CS model

The Magneli phases all have the CS displacement vector in the plane perpendicular to the 3.85 Å projection axis. However, there also exists a number of perovskite-derived CS structures in which the CS vector has a component along the projection axis. These are the so-called block or column structures, first elucidated by Wadsley and co-workers [19], which contain two sets of CS planes perpendicular to one another. If the 3.8 Å projection axis common to these structures is labelled b, then the CS vectors are of the type $\frac{1}{2}[110]_p$ and $\frac{1}{2}[011]_p$. As an illustration, the MoO_3 structure can be derived from the ReO_3 structure by alternate application of these two CS vectors on $(100)_p$ planes as shown in Fig. 3(a). The operation $\frac{1}{2}[011](100)_p$ results in a higher O/M ratio while the operation $\frac{1}{2}[1\bar{1}0](100)_p$ lowers the O/M ratio (= reduction). The combination shown in Fig 3(a) leaves the stoichiometry unchanged. Application of the CS vector $\frac{1}{2}[110]_p$ to $(101)_p$ and $(201)_p$ planes is shown in Figs. 3(b) and (c), respectively.

The operations shown in Figs 3(b) and (c) can be combined to give the CS operation $\frac{1}{2}[110](704)_p$ as shown in Fig. 4(a). Periodic application of this operation generates a model with the correct cell dimensions and symmetry for $PbMnO_{2.75}$ (including calculated a and c cell parameters that are both smaller than the experimental values, consistent with expected trends due to metal–metal repulsions at the CS planes). In this model, conforming to space group $A2/m$, Mn was ordered into the octahedra and Pb was located in the available A-type cavities. Refinement of the Pb and Mn coordinates gave a good fit to the powder XRD pattern. However, the calculated unit-cell composition, $Pb_{38}Mn_{60}O_{174}$, had a Pb/Mn ratio quite different from 1:1. This problem was resolved using difference Fourier synthesis, which showed high electron density in the CS planes, very close ($\leqslant 1$ Å) to those oxygen atoms not involved in octahedral corner-sharing. At the same time, the refinement showed that the Mn atoms associated with these oxygen atoms underwent large displacements away from them. This suggested that the non-bridging

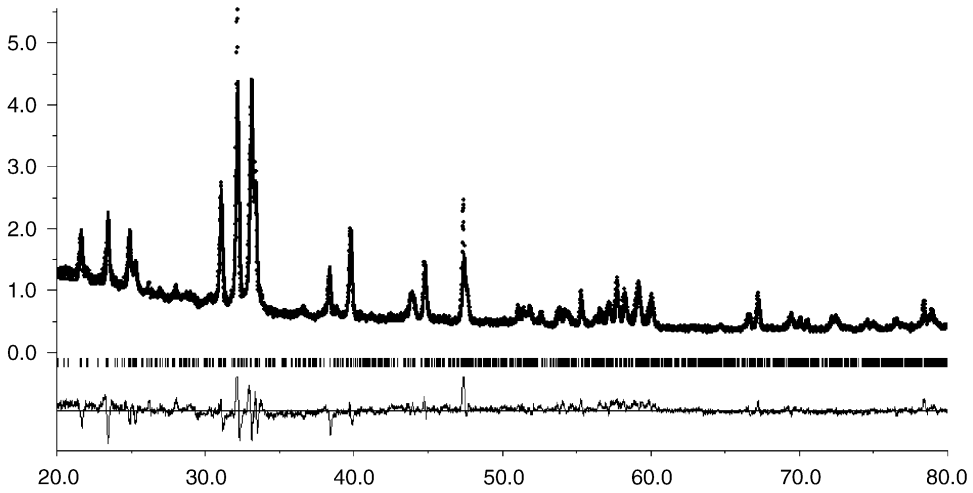

Fig. 5. Measured (dots) and calculated (line) powder XRD pattern for $PbMnO_{2.75}$. Positions of Bragg reflections as well as difference plot from Rietveld refinement are shown,

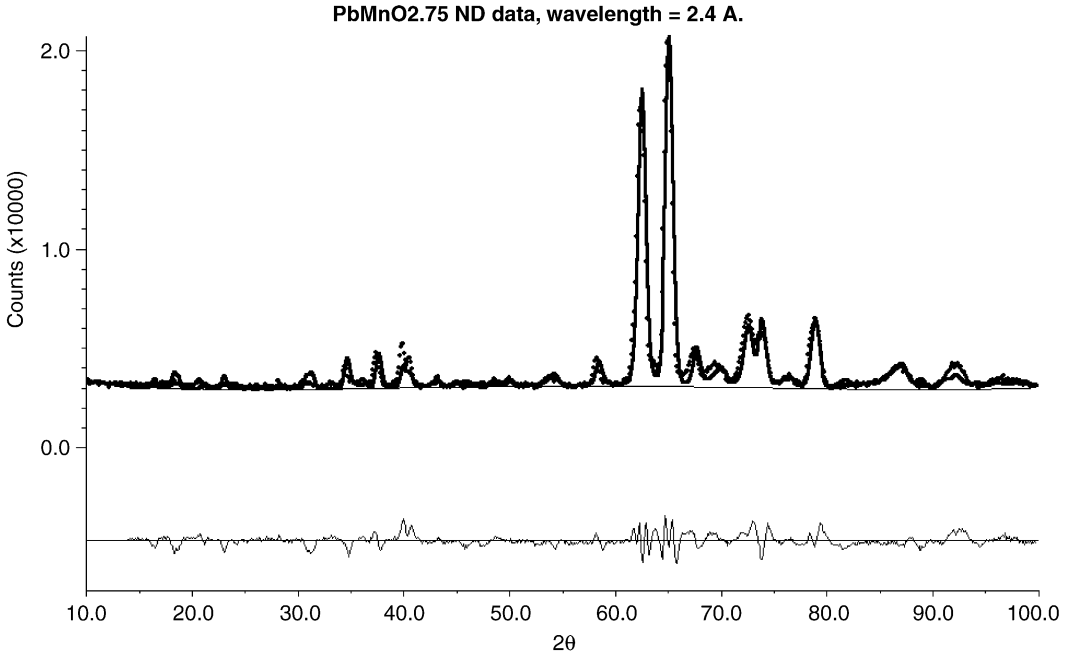

Fig. 6. Measured (dots) and calculated (line) powder ND pattern for $PbMnO_{2.75}$. Shown below is the difference plot from Rietveld refinement.

oxygen atoms do not form part of the structure, as shown in Fig. 4(b). These oxygen atoms were removed and Pb atoms were added in the positions indicated from the difference Fourier maps, as shown in Fig. 4(c).

Refinement of the Pb and Mn atoms using the powder XRD data resulted in convergence at $Rw_p = 8.8\%$, $R_b = 5.3\%$. A comparison of measured and calculated powder XRD patterns is shown in Fig. 5. No attempt was made to refine the oxygen atoms, of which there are 40 independent atoms in the unit cell. They were left at the ideal perovskite positions calculated from the matrix relating the structure to that of perovskite/ReO_3. The general validity of the model was confirmed both by the sensible Mn–O and Pb–O bond lengths and by the reasonable fit to the powder ND data, shown in Fig. 6. Refinement of the ND profile parameters gave $Rw_p = 6.7\%$, $R_b = 3.0\%$. The atomic coordinates are reported in Table 2.

3.4. Description of structure

A polyhedral representation of the structure of $PbMnO_{2.75}$ projected along [010] is shown in Fig. 7. It comprises blocks of perovskite-type structure which are

Table 2
Atomic coordinates for $PbMnO_{2.75}$ prepared at 7.8 GPa and 880°C

Atom	x	y	z	Atom	x	y	z
MN1	0.992	0.0	0.172	O1	0.019	0.0	0.142
MN2	0.052	0.0	0.103	O2	0.075	0.0	0.066
MN3	0.102	0.0	0.017	O3	0.132	0.0	0.990
MN4	0.226	0.0	0.228	O4	0.123	0.0	0.170
MN5	0.252	0.0	0.157	O5	0.179	0.0	0.094
MN6	0.323	0.0	0.086	O6	0.236	0.0	0.019
MN7	0.360	0.0	0.004	O7	0.226	0.0	0.198
MN8	0.475	0.0	0.205	O8	0.283	0.0	0.123
MN9	0.521	0.0	0.135	O9	0.339	0.0	0.047
MN10	0.578	0.0	0.057	O10	0.387	0.0	0.151
MN11	0.690	0.0	0.260	O11	0.443	0.0	0.075
MN12	0.725	0.0	0.194	O12	0.500	0.0	0.000
MN13	0.788	0.0	0.122	O13	0.490	0.0	0.179
MN14	0.839	0.0	0.049	O14	0.547	0.0	0.104
MN15	0.952	0.0	0.243	O15	0.604	0.0	0.028
				O16	0.594	0.0	0.207
PB1	0.151	0.5	0.120	O17	0.651	0.0	0.132
PB2	0.212	0.5	0.055	O18	0.707	0.0	0.056
PB3	0.413	0.5	0.103	O19	0.698	0.0	0.236
PB4	0.466	0.5	0.028	O20	0.754	0.0	0.160
PB5	0.627	0.5	0.158	O21	0.811	0.0	0.085
PB6	0.675	0.5	0.089	O22	0.858	0.0	0.189
PB7	0.727	0.5	0.018	O23	0.915	0.0	0.113
PB8	0.886	0.5	0.135	O24	0.971	0.0	0.038
PB9	0.937	0.5	0.061	O25	0.962	0.0	0.217
PB10	0.000	0.5	0.000	O26	0.991	0.5	0.178
PB11	0.359	0.5	0.176	O27	0.047	0.5	0.104
PB12	0.174	0.0	0.297	O28	0.104	0.5	0.028
PB13	0.422	0.0	0.269	O29	0.198	0.5	0.236
PB14	0.084	0.5	0.186	O30	0.255	0.5	0.160
				O31	0.311	0.5	0.085
				O32	0.368	0.5	0.009
				O33	0.462	0.5	0.217
				O34	0.519	0.5	0.141
				O35	0.575	0.5	0.066
				O36	0.670	0.5	0.274
				O37	0.726	0.5	0.198
				O38	0.783	0.5	0.123
				O39	0.839	0.5	0.047
				O40	0.934	0.5	0.255

E.s.d. values = 0.007 for Mn x and z and 0.002 for Pb x and z.
Oxygen coordinates and temperature factors not refined ($B = 0.5$ for all atoms).

periodically displaced relative to one another across planes parallel to $(704)_p$. The displacement vector, $\frac{1}{2}[110]_p$, corresponds to an octahedral edge. The structure is simply described as a perovskite CS structure with the CS operation $= \frac{1}{2}[110](704)_p$. The relationships between the cell parameters of the CS phase and the cubic perovskite subcell are: $a = 4a_p - 7c_p$, $b = b_p$, $c = 3a_p + 8c_p$. Transposing these equations gave expressions for calculating the ideal coordinates of all atoms in the CS phase.

At the CS boundaries, the CS operation formally converts the exclusive corner-sharing of octahedral vertices as in perovskite to a mixture of edge-sharing and isolated vertices (non-bridging). The non-bridging octahedral sites are vacant in $PbMnO_{2.75}$, generating pseudo-hexagonal channels parallel to [010], and converting the octahedral coordination of manganese to square-pyramidal coordination for the manganese atoms Mn(4), Mn(8), Mn(11) and Mn(15) in Table 2. This type of coordination has been previously reported for Mn^{3+} in the oxygen-deficient perovskite phases $Ca_2Mn_2O_5$ [20] and $Sr_2Mn_2O_5$ [21]. The MnO_5 square pyramids share edges with adjacent octahedra in the CS planes for Mn(4), Mn(11) and Mn(15), while $Mn(8)O_5$ square pyramids form edge-shared chains along [010].

Pb atoms Pb(11) to Pb(14) in Table 2 occupy sites in the pseudo-hexagonal channels such that they have square planar coordination. The Pb atoms are slightly displaced from the square of oxygen atoms, as in tetragonal PbO [22]. The PbO_4 pyramidal units share

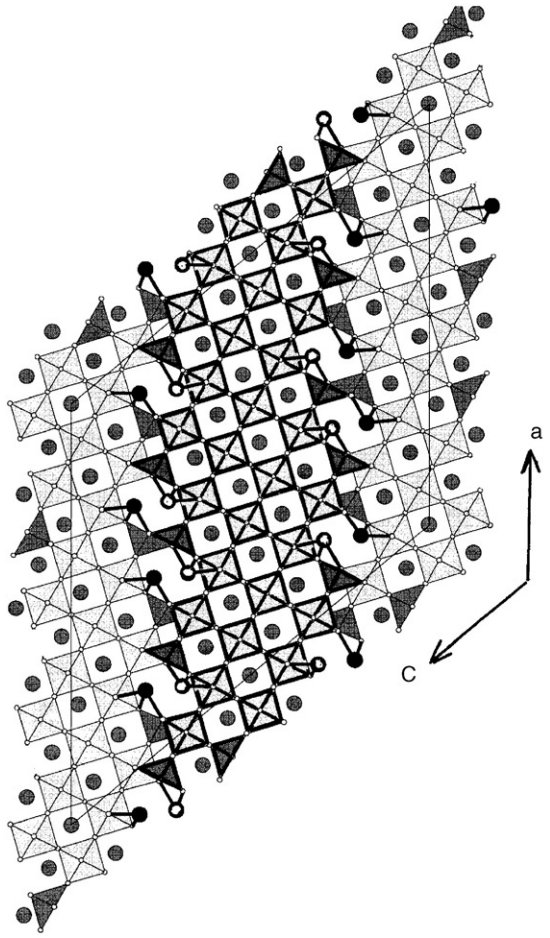

Fig. 7. [010] projection of the structure for $PbMnO_{2.75}$. Light and dark outlined octahedra are at $y = 0$ and 0.5, respectively. Open and filled circles represent Pb atoms at $y = 0$ and 0.5.

edges with MnO_5 square pyramids, giving the same topology as in tetragonal PbO. Similar pyramidal coordination for Pb^{2+} occurs for half of the lead atoms in the lead manganite $Pb_3Mn_7O_{15}$ [8]. The location of the Pb atoms in the channels provides room for the $6s^2$ lone pairs as illustrated in Fig. 4(c).

In $PbMnO_{2.75}$ the cuboctahedral *A*-sites of the perovskite blocks are also occupied by lead atoms, Pb(1) to Pb(10) in Table 2. Occupation of the centers of the *A* sites would give 12 Pb^{2+}–O distances of ~ 2.8 Å. The metal atom coordinates refinement showed that the lead atoms are displaced from the centers of the cuboctahedra to give typically 4–6 shorter Pb–O distances, as observed for example in ferroelectric $PbTiO_3$ perovskite [23]. The refined Mn and Pb positions reveal some short distances. In particular, MnO_5 square pyramids and MnO_6 octahedra which share edges in the CS boundaries have Mn–Mn separations of 2.75–2.8 Å and several distances between the four coordinated Pb atoms in the pseudo-hexagonal channels and the surrounding Mn atoms are ~ 3.1 Å. Similar metal–metal distances were found in $Pb_3Mn_7O_{15}$ (8).

The unit-cell composition calculated from the structural model is $Pb_{54}Mn^{3+}_{32}Mn^{4+}_{28}O_{158}$, where the Mn^{3+}/Mn^{4+} ratio shown is required for charge balancing. The calculation assumes full ordering of Mn in the octahedral framework and Pb in the cavity sites. This compares reasonably well with the starting composition of $Pb_{60}Mn^{3+}_{30}Mn^{4+}_{30}O_{165}$. A closer match to the experimental composition can be obtained if some substitution of lead for manganese occurs in the framework sites. The most likely manganese sites for the substitution to occur are the square pyramidal sites in the CS planes. Substitution of lead in these sites would generate small elements of the tetragonal PbO structure. In fact, a small reduction in the R factors were obtained when some Pb substitution was introduced at the sites Mn(4), Mn(8), Mn(11) and Mn(15). However, the large unit cell with severe peak overlap prevented an accurate determination of site substitutions from Rietveld refinement of the powder data. More detailed elucidation of the structural details in $PbMnO_{2.75}$ will require single crystals to be obtained.

The CS plane orientation of $(704)_p$ found for $PbMnO_{2.75}$ is a high-order plane for the perovskite structure and there is no clear reason for this being a unique CS plane for the Pb–Mn–O system. Indeed, in on-going high-pressure studies involving variation of Pb/Mn and Mn^{3+}/Mn^{4+} ratios, we find systematic changes in the powder patterns of the products that are suggestive of changes of CS plane orientation and/or CS plane spacings, such as that occurs in the "swinging" CS region of the TiO_{2-x} phase system [24]. Elucidation of the structural complexity of this system will require initially electron microscopy and diffraction studies to determine the CS plane orientations and spacings in the different preparations. It is hoped that pure phases can be prepared with lower index CS planes that will lead to smaller cells and thus to the opportunity to obtain more detailed information on the coordination and polyhedral distortions from powder refinements. The potential for controlling physical properties with control of the geometry of the CS planar defects is a strong incentive for further studies in this field.

Acknowledgments

We thank Alan Hewat and Thomas Hansen at ILL for the neutron diffraction data collections and Pierre Bordet at CNRS Grenoble for help with the XRD data collections. Thanks to Mark Pownceby for reviewing the manuscript.

References

[1] A. Moreo, S. Yunoki, E. Dagotto, Science 283 (1999) 2034.
[2] S. Mori, C.H. Chen, S.-W. Cheong, Nature 392 (1998) 473.
[3] A. Asamitsu, Y. Morimoto, Y. Tomioka, T. Arima, Y. Tokura, Nature 373 (1995) 407.
[4] S. Hashimoto, H. Iwahara, Mater. Res. Bull. 35 (2000) 2253.
[5] J.L. Garcia-Munoz, C. Frontera, M.A.G. Aranda, A. Llobet, C. Ritter, Phys. Rev. B 63 (2001) 064415.
[6] A. Teichert, H. Muller-Buschbaum, Z. Anorg. Allg. Chem. 598/599 (1991) 319.
[7] J.E. Post, D.L. Bish, Am. Mineral. 74 (1989) 913.
[8] B. Darriet, M. Devalette, B. Latourrette, Acta Crystallogr. Sect. B 34 (1978) 3528.
[9] B. Latourrette, M. Devalette, F. Guillen, C. Fouassier, Mater. Res. Bull. 13 (1978) 567.
[10] T. Atou, H. Chiba, K. Ohoyama, Y. Yamaguchi, Y. Syono, J. Solid State Chem. 145 (1999) 639.
[11] C. Bougerol, M.F. Gorius, P. Bordet, I.E. Grey, Acta. Crystallogr. Sect. A 58 (suppl) (2002) C23.
[12] J. Akimoto, Y. Gotoh, Y. Ossawa, Acta Crystallogr. Sect. C 50 (1994) 160.
[13] T.C. Hansen, P. Convert, Materials Science Forum EPDIC7, Part 1, 294 (2001) 378.
[14] R.J. Hill, C.J. Howard, J. Appl. Crystallogr. 18 (1985) 173.
[15] D.B. Wiles, R.A. Young, J. Appl. Crystallogr. 14 (1981) 149.
[16] A.A. Bush, A.V. Titov, B.I. Al'shin, Yu.N. Venevtsev, Russ. J. Inorg. Chem. 22 (8) (1977) 1211.
[17] L.A. Bursill, B.G. Hyde, J. Solid State Chem. 4 (1972) 430.
[18] A. Magneli, Acta Crystallogr. 6 (1953) 495.
[19] A.D. Wadsley, Acta Crystallogr. 14 (1961) 664.
[20] K.R. Poeppelmeier, M.E. Leonowicz, J.C. Scanlon, J.M. Longo, W.B. Yelon, J. Solid State Chem. 45 (1982) 71.
[21] V. Caignaert, N. Nguyen, M. Hervieu, B. Raveau, Mater. Res. Bull. 20 (1985) 479.
[22] P. Boher, P. Garnier, J.R. Gavarri, A.W. Hewat, J. Solid State Chem. 57 (1985) 343.
[23] G. Shirane, R. Pepinsky, B.C. Frazer, Acta Crystallogr. 9 (1956) 131.
[24] L.A. Bursill, B.G. Hyde, D.K. Philp, Philos. Mag. 23 (1970) 150.